IEEE Access
Multidisciplinary ⋮ Rapid Review ⋮ Open Access Journal

Received 4 January 2024, accepted 21 January 2024, date of publication 25 January 2024, date of current version 1 February 2024.

Digital Object Identifier 10.1109/ACCESS.2024.3358456

RESEARCH ARTICLE

Identification of Equivalent Circuit Parameters for Proton Exchange Membrane (PEM) Electrolyzer Engineering Models

XINKE MAO[1], YIZHI TIAN[1], AIMEI YANG[2], AND GAOHANG ZHANG[1]
[1]School of Electrical Engineering, Xinjiang University, Ürümqi 830000, China
[2]Goldwind Science and Technology Company Ltd., Ürümqi 830000, China

Corresponding author: Yizhi Tian (torsionscale@163.com)

This work was supported in part by the Natural Science Foundation of Xinjiang Uygur Autonomous Region under Grant 2022D01C364, and in part by the Key Research and Development Program of Xinjiang Uygur Autonomous Region under Grant 2022B01016.

ABSTRACT This paper addresses the problem of underestimated temperature measurements in practical proton exchange membrane (PEM) electrolyzer engineering due to heat losses by enhancing the existing second-order RC equivalent circuit model of PEM electrolyzers. We present a novel engineering circuit model for PEM electrolyzers, incorporating the effects of heat losses from gases and pipelines. The objective is to enhance the model's ability to predict electrolyzer performance and align control strategies with the realities of engineering practice. However, the PEM electrolyzer model is complex, being time-varying and nonlinear due to multi-physics field coupling. The parameters of the equivalent circuit are changed by the electrical energy input and its own state. To tackle the problem of parameter variation, firstly, a recursive identification algorithm is employed to estimate the internal equivalent circuit parameters of the engineering model. Then, the additional resistance is fitted according to the relationship between heat loss and current to complete the engineering circuit model identification. Finally, using MATLAB to construct an engineering model and validate the effectiveness of the proposed identification algorithm.

INDEX TERMS Proton exchange membrane (PEM), engineering circuit mode, parameter identification, recursive identification algorithm, curve fitting, system simulation.

I. INTRODUCTION

Due to the increasing demand for global energy supply and the growing significance of environmental and climate issues, green, low-carbon, and sustainable development has gained worldwide prominence. Hydrogen, owing to its environmental friendliness, high energy density, and wide range of sources, is regarded as a promising energy source [1]. Hydrogen production methods include fossil fuel-based production, industrial byproduct utilization, and water electrolysis. Among these methods, water electrolysis stands out as the cleanest. As the installed capacity of renewable energy continues to rise, the integration of renewable energy and electrolysis technology is set to emerge as the predominant approach for producing green hydrogen in the future [2]. Water electrolysis technology encompasses various techniques: alkaline electrolysis (AEL), proton exchange membrane electrolysis (PEM), solid oxide electrolysis (SOEC), and anion exchange membrane electrolysis (AEM). Among these, PEM electrolysis technology features high power density, exceptional electrolysis efficiency, superior hydrogen purity, rapid system response, and great flexibility. It is well-suited to accommodate the intermittent, stochastic, and fluctuating nature of renewable energy generation. As a result, PEM electrolysis has garnered extensive attention in both the research and industrial sectors [3], [4]. Nafion excels as a Proton Exchange Membrane (PEM), enhancing PEM electrolysis cell performance with superior proton conductivity, chemical stability, mechanical flexibility, water management capabilities, and widespread commercial availability [5].

The associate editor coordinating the review of this manuscript and approving it for publication was Behnam Mohammadi-Ivatloo.

Developing an accurate model for a PEM electrolyzer is crucial for researchers to investigate and analyze significant issues such as design, control, evaluation, and more under different operating conditions. Atlam utilized experimental data to construct a PEM electrolyzer circuit model, deducing the relationship between input electrical energy and hydrogen production rate [6]. Damien Guilbert extending from steady-state circuitry, considered abrupt changes in current and employed least-square regression algorithms to fit capacitance and resistance parameters, resulting in a dynamic circuit model [7]. Jian Dang constructed a transient model for the PEM electrolyzer using differential equations and equivalent activation overpotential [8]. Ángel Hernández-Gómez further optimized the differential equations for cathode and anode activation overpotentials, forming a static-dynamic adaptive model [9]. Although the models developed by literatures [6], [7], [8], and [9], effectively capture the I-V relationship of the PEM electrolyzer, they do not adequately reflect the physical and chemical principles of the internal components. In recent years, emerging electrochemical models have built upon the basis of equivalent circuit models, introducing enhancements like dynamic sub-models and thermodynamic sub-models. Such models further elucidate operational mechanisms, offering reasonable explanations for electrode polarization and mass transfer processes within the PEM electrolyzer. The model established by García-Valverde et al. considers the influence of temperature on the PEM electrolyzer, but it is relatively straightforward and does not incorporate the effect of pressure [11]. Abdin et al. considered concentration overpotentials but encountered difficulties in estimating parameters like electro-osmotic drag [12]. Tevfik and Faruk modeled the entire PEM electrolyzer system, encompassing water circulation and cooling systems [13]. Afshari et al. delved deeper into mass transfer processes involving gases and water, including gas crossover phenomena and water transport [14]. While electrochemical models for PEM electrolyzers effectively simulate polarization and mass transfer processes, these models are built upon experimental PEM electrolyzer foundations and do not account for heat losses in practical engineering contexts [11], [12], [13], [14].

Since the parameters of the PEM electrolyzer are changed by the input electrical energy and its own state, it is necessary to employ identification methods to estimate these real-time changing parameters. Identification methods primarily fall into two categories: numerical identification algorithms and heuristic optimization algorithms. Rahul Khajuria employed the honey badger algorithm for parameter identification of seven parameters in the PEM electrolyzer cell. A comparison with heuristic algorithms such as PSO and GWO demonstrated the superiority of the honey badger algorithm [15]. Toghyani et al. utilized the Taguchi algorithm to optimize parameters and obtain the optimal working conditions [16]. Khajuria et al. applied metaheuristic algorithms to identify six unknown parameters of the PEM electrolyzer [17]. While heuristic algorithms often demonstrate superior adaptability to avoid local optima, their reliance on empirical knowledge and intuition introduces variability in results across different runs, lacking a guarantee of solution accuracy. In contrast, numerical algorithms, with their rigorous mathematical foundations, prove invaluable in scientific computations and precision-demanding engineering applications. In this paper, we employ a multi-innovation least squares identification algorithm to identify the equivalent circuit parameters of a PEM electrolyzer. This algorithm improves the convergence speed problem of numerical algorithms while avoiding the local optimization problem of heuristic algorithms.

To facilitate more convenient measurement of PEM electrolyzer data in the experimental environment, independent drain and outlet ports were set up, each equipped with temperature measurement holes. However, in practical engineering scenarios, to ensure internal pressure within the PEM electrolyzer, it is designed as a sealed container, with the air outlet and water outlet combined into a single outlet. The oxygen produced is discharged along with the circulating water through the anode outlet, while the hydrogen generated is released through the cathode outlet along with a small amount of circulating water. The gas discharged with the circulating water carries a non-negligible amount of heat, and the circulating water also generates a non-negligible amount of energy loss in the pipeline; however, the experimental model does not consider the aforementioned heat loss. Therefore, based on the electrochemical model, this paper introduces a model tailored for engineering applications. The model equates the heat losses in gas and circulating water to an external additional resistor within the framework of a second-order RC circuit. It employs a recursive identification algorithm to estimate internal equivalent circuit parameters and utilizes a curve-fitting method to model the external additional resistor. Finally, the reliability of the engineering model and the accuracy of the identification method are validated through simulation experiments. This enhances the predictive capability of the PEM electrolyzer's behavior in practical engineering scenarios, offering valuable insights for control system design.

II. EQUIVALENT CIRCUIT MODEL OF PEM ELECTROLYZE

Constructing an equivalent circuit model for a PEM electrolyzer is a prerequisite for characterizing its electrochemical properties and studying control strategies. However, due to structural differences between PEM electrolyzers used in experimental settings and practical engineering scenarios, their corresponding equivalent circuit models are also different. Case (a) in Fig. 1 illustrates the schematic diagram of a circulating water system for a PEM electrolyzer in an experimental environment. In this setup, the generated hydrogen, oxygen, and circulating water are discharged separately through the cathode outlet, anode outlet, and water outlet, respectively. Additionally, temperature measurement ports are present in both the cathode and anode. While the circulating water supply system of the PEM electrolyzer in actual engineering, as shown in case (b) of Fig. 1, cathode circulating water and hydrogen exit jointly from the

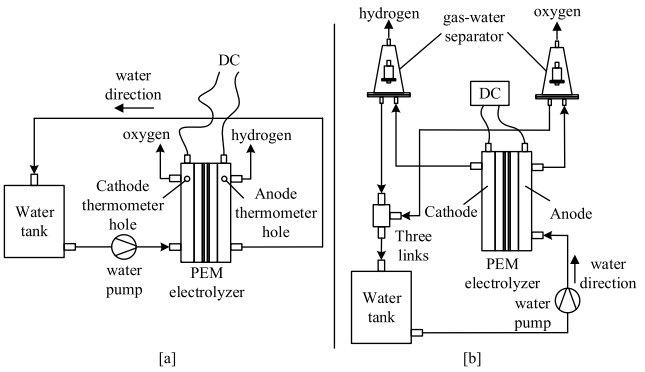

FIGURE 1. Circulating water supply system for PEM electrolyzer in experimental setting (a) and engineering (b).

cathode outlet, while anode circulating water and oxygen exit together.

The circulating water supply system equipment for the PEM electrolyzer in the practical engineering context includes one PEM electrolyzer, one water tank, two gas-water separators, one water pump, one tee, and some silicone tubes, as shown on the right side of Fig 1. When the system is running, the deionized water passes through the water inlet, the pole plate flow field, and the porous transport layer to the anode side of the membrane electrode, and is decomposed into oxygen, electrons, and protons under the action of electric energy and catalyst. Some of the oxygen and deionized water travel through the anode outlet and pipeline to the gas-water separator. The separated deionized water is directed to the water tank via the three-way valve. On the cathode side, electrons flow through the membrane electrode and electrode plate, returning to the external circuit to provide the driving force for the electrolytic reaction. Protons and a small amount of deionized water traverse the proton exchange membrane to reach the cathode side. In the presence of catalysts, protons combine with electrons from the external circuit to generate hydrogen gas. The generated hydrogen gas, accompanied by a small amount of deionized water, passes through the porous transport layer and the bipolar plate flow field to reach the cathode outlet. This mixture then travels through the pipeline to the gas-water separator, where the separated hydrogen gas is collected in a hydrogen storage unit. The deionized water passes through the three-way valve and enters the water tank.

A. STRUCTURE AND EQUIVALENT CIRCUIT OF PEM ELECTROLYZER BASED ON EXPERIMENTAL ENVIRONMENT

The commonly used equivalent circuit model of the PEM electrolyzer is the second-order RC circuit model, which can simulate the voltage distribution and dynamic characteristics of the PEM electrolyzer in the experimental environment. The overall operating voltage of the equivalent circuit of the PEM electrolyzer in the experimental environment consists of reversible voltage U_{rev}, cathode activation overvoltage U_{act}, ohmic overvoltage U_{ohm}, and the expression is as follows [9], [10], [12], and [13]:

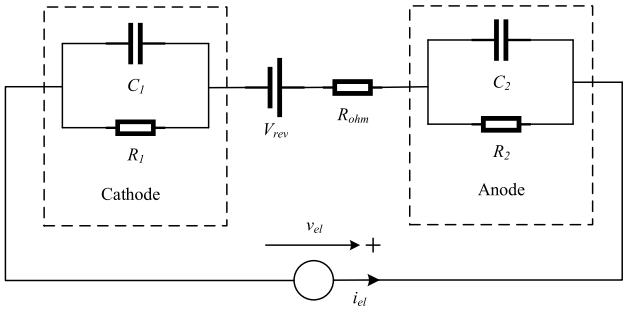

FIGURE 2. Equivalent circuit of PEM electrolyzer.

$$U_{cell} = U_{rev} + U_{act.c} + U_{act.a} + U_{ohm} \tag{1}$$

The equivalent circuit model corresponding to (1) is illustrated in Fig. 2. The reversible voltage U_{rev} signifies the fundamental voltage required for the electrolysis of water, while the Ohmic resistance R_{ohm} characterizes the resistance generated by protons passing through the proton exchange membrane and the hindrance of current by the electrode plates. C_1 and C_2 represent the equivalent capacitance of the cathode and anode, respectively, induced by the double-layer effects at the cathode and anode. R_1 is the cathode resistance, representing the resistance causing Gibbs energy and heat loss at the anode, while R_2 is the anode resistance, representing the resistance causing heat loss at the cathode. The time constants τ_1 and τ_2 are used to denote the time required for the dynamic behavior of the cathode and anode in the PEM electrolyzer.

The reversible overpotential U_{rev} is the minimum voltage required for the electrolysis of water, representing the smallest voltage necessary to convert electrical energy into chemical energy. It is derived from the Nernst equation [12].

$$U_{rev} = 1.229 - 0.9 \times 10^{-3}(T_{cell} - T_0) + \frac{RT_{cell}}{2F} \ln\left(\frac{p_{H_2}(p_{O_2})^{0.5}}{p_{H_2O}}\right) \tag{2}$$

where R is the ideal gas constant, T_{cell} is the operating temperature of the electrolyzer, F is the Faraday constant, P_{H_2} and P_{O_2} represent the partial pressures of the gas products hydrogen and oxygen respectively, and P_{H_2O} represents the partial pressure of water at the cathode and anode. T_0 signifies the external environmental pressure. Activation overvoltage is generated by electrochemical polarization. It signifies a voltage shift due to the sluggishness of electrochemical reactions, which is required to maintain the motion of protons and electrons. It can be mathematically expressed using the Butler-Volmer equation [13]:

$$U_{act} = U_{act}^{an} + U_{act}^{cat} = \frac{RT}{\alpha_{an}F} \sinh^{-1}\left(\frac{i}{2i_{0,an}}\right) + \frac{RT}{\alpha_{cat}F} \sinh^{-1}\left(\frac{i}{2i_{0,cat}}\right) \tag{3}$$

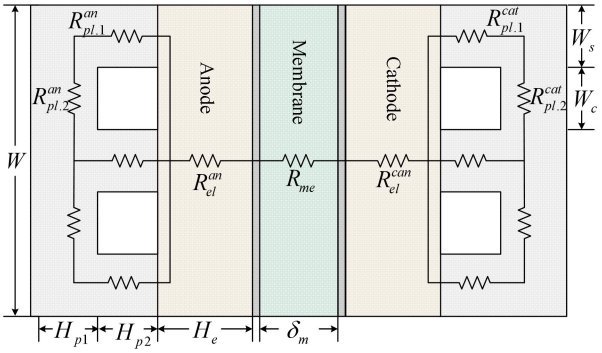

FIGURE 3. PEM electrolyzer ohmic resistance distribution.

where i is the current density, α_{cat} and α_{an} are the cathode and anode charge transfer coefficients, and $i_{0,cat}$ and $i_{0,an}$ are the cathode and anode exchange current densities. The cathode and anode equivalent time constants τ_1 and τ_2 are estimated as follows [9]:

$$\begin{cases} \tau_{cat} = 1.1562 \times \exp\left[\dfrac{-(I_{cell} - 4.2672)^2}{0.09487}\right] + 0.606 \\ \tau_{an} = 0.1 \times \tau_{cat} \end{cases} \tag{4}$$

Then, by relating the time constants to the resistances, the equivalent capacitance of the cathode and anode can be obtained:

$$\begin{cases} \tau_{cat} = C_1 \times R_1 = C_1 \times \left(\dfrac{U_{act}^{cat}}{i_{cell}}\right) \\ \tau_{an} = C_2 \times R_2 = C_2 \times \left(\dfrac{U_{act}^{an}}{i_{cell}}\right) \end{cases} \tag{5}$$

In Fig. 3, the Ohmic overpotential encompasses the overpotential arising from the hindrance of protons by the proton exchange membrane and the overpotential stemming from the impedance caused by the bipolar plates and gas diffusion layers to the flow of electrons. The expressions are as follows:

$$U_{ohm} = R_{ohm} \times i_{el} = (R_{el} + R_{pl} + R_{me}) i_{el} \tag{6}$$

In Equation (6), R_{pl}, R_{el}, and R_{me} respectively denote the resistances imposed on electron transport by the electrode plates, the porous transport layer, and the proton exchange membrane. These can be expressed as [14]:

$$\begin{cases} R_{pl.1}^{an} = \dfrac{\rho_{pl}^{an}(W_s + W_c)}{LH_{p1}} \; R_{pl.2}^{an} = \dfrac{\rho_{pl}^{an} W_s}{LH_{p2}} \\ R_{pl.1}^{cat} = \dfrac{\rho_{pl}^{cat}(W_s + W_c)}{LH_{p1}} \; R_{pl.2}^{cat} = \dfrac{\rho_{pl}^{cat} W_s}{LH_{p2}} \\ R_{el}^{an} = \dfrac{\rho_{eff} H_e}{LW} R_{el}^{can} = \dfrac{\rho_{eff} H_e}{LW} \\ \rho_{eff} = \dfrac{\rho_{el}}{(1-\varepsilon)^{1.5}} \end{cases} \tag{7}$$

In Equation (7), where ρ_{pl}^{an} and ρ_{pl}^{cat} represent the resistivity of the two electrode plates, respectively. W_s denotes the width of the flow field channel supporting the electrode plates, W_c represents the width of the flow field channel, H_{p1} and H_{p2} respectively denote the thickness of the cathode and anode electrode plates as well as the height of the flow field channel. ρ_{eff} represents the effective resistance of the gas diffusion layer. L is the length of the electrolysis cell, W is the width of the electrolysis cell, H_e is the width of the porous transport layer, and ρ_{el} and ε respectively denote the resistance and porosity of the gas diffusion layer for the cathode and anode. The resistance of the proton exchange membrane is given by [16]:

$$R_{me} = \frac{\delta_m}{\sigma_m} \tag{8}$$

where δ_m is the thickness of the proton exchange membrane and σ_m is the proton exchange membrane conductivity. An empirical formula is provided as follows [13]:

$$\sigma_{me} = (0.005139\lambda - 0.00326) \exp(1268(\frac{1}{303} - \frac{1}{T_{cell}})) \tag{9}$$

where λ represents the wetness of the proton exchange membrane, and it can be empirically expressed as:

$$\lambda = 0.08533 T_c - 6.77632 \tag{10}$$

The above model represents a PEM electrolyzer cell in an experimental environment. Due to the presence of temperature measurement holes in the experimental setup and the separate discharge of circulating water and gas, the temperature measured at these holes is considered the electrolyzer cell temperature, and any temperature deviation can be considered negligible. However, in engineering applications, PEM electrolyzers experience significant heat losses that cannot be ignored. Therefore, the model developed in the experimental environment is not suitable for practical engineering applications, and there is a need to establish an equivalent circuit model that is appropriate for engineering scenarios.

B. MODEL STRUCTURE AND EQUIVALENT CIRCUIT OF PEM ELECTROLYZER BASED ON ENGINEERING PRACTICE

There are two main differences between the PEM electrolyzer in actual engineering and the one in the experimental environment. Firstly, in the engineering setup, the PEM electrolyzer is a sealed container and does not have temperature measurement holes, necessitating temperature measurements at the gas-water separator outlet, which results in some heat loss through the pipelines. Secondly, in the experimental model, the water temperature is approximated as the temperature of the PEM electrolyzer, without accounting for the heat within the gases. The above two points indicate that the model in the experimental setting deviates significantly from the actual project.

Temperature is a crucial factor influencing the performance of PEM electrolyzers. Parameters such as thermal equilibrium voltage, proton exchange membrane conductivity, and exchange current density are significantly affected by temperature variations [8]. The PEM electrolyzer model developed

under laboratory conditions does not account for the heat in the gases and the heat dissipation through pipelines, which leads to a discrepancy between the measured temperature and the actual temperature in real engineering applications. If temperature data with certain deviations are used for simulating, predicting, and controlling engineering processes, it can lead to reduced hydrogen production efficiency, at best. At worst, it can result in damage to components such as the membrane electrode. In order to make the model compatible with actual temperature for engineering measurements, we introduce an engineering-specific model.

1) MODEL STRUCTURE AND EQUIVALENT CIRCUIT OF PEM ELECTROLYZER BASED ON ENGINEERING PRACTICE

Modeling assumptions:

1) The heat generated by the Joule heating effect at the cathode and anode is approximately equal.
2) The electrolyzer has excellent thermal insulation, and there is no heat exchange between the equipment itself and the external environment.
3) Throughout the entire experimental duration, the heat flow per unit time is equal to the total heat generated divided by the total time.

If the resistances at the cathode and anode of the PEM electrolyzer are approximately equal, then the heat generated at each electrode due to Joule heating is roughly equal. Consequently, each electrode contributes half of the heat generated by the Joule heating effect. The heat generated at the anode and cathode per unit time can be determined using Ohm's law:

$$\dot{Q}_{all}^{an} = \dot{Q}_{all}^{cat} = \frac{1}{2} I_{cell}^2 R_{total} \tag{11}$$

where R_{total} represents the total equivalent resistance within the electrolyzer. The heat discharged from the anode into the circulating water per unit time is given by:

$$\begin{aligned} \dot{Q}_{H_2O}^{an} &= C_{H_2O} \dot{N}_{H_2O,out}^{an} (T_{cell}^{an} - T_0) \\ &= C_{H_2O} (\dot{N}_{H_2O,in} - \dot{N}_{H_2O,con} - \dot{N}_{H_2O,mem}) (T_{cell}^{an} - T_0) \end{aligned} \tag{12}$$

The heat discharged from the anode into the oxygen gas per unit time is given by:

$$\dot{Q}_{O_2} = C_{O_2} \dot{N}_{O_2} (T_{cell}^{an} - T_0) \tag{13}$$

The heat discharged from the anode per unit time is equal to the sum of the heat discharged into the circulating water and the heat discharged into the oxygen:

$$\begin{aligned} \dot{Q}_{out}^{an} &= \dot{Q}_{H_2O}^{an} + \dot{Q}_{O_2} \\ &= (C_{H_2O} \dot{N}_{H_2O,out}^{an} + C_{O_2} \dot{N}_{O_2}) (T_{cell}^{an} - T_0) \end{aligned} \tag{14}$$

where, C_{H_2O} and C_{O_2} represent the molar heat capacities of water and oxygen gas. Additionally, $\dot{N}_{H_2O,out}^{an}$, $\dot{N}_{H_2O,in}$, $\dot{N}_{H_2O,con}$, and $\dot{N}_{H_2O,mem}$ denote the molar mass of water discharged from the anode per unit time, the molar mass of water entering the system per unit time, the molar mass of water consumed during the electrolysis process per unit time, and the molar mass of water transferred from the anode side to the cathode side through the proton exchange membrane (via processes like electrodialysis and diffusion). T_0 and T_{cell}^{an} represent room temperature and the anode temperature of the electrolyzer, respectively. The anode heat is calculated by subtracting the heat generated by the anode electrical energy from the heat of the anode outlet drainage and exhaust, and then the anode temperature is reverse-calculated using the heat calculation formula:

$$T_{cell}^{an} = \frac{\int_{t_1}^{t_2} \left(\dot{Q}_{all}^{an} - \dot{Q}_{out}^{an} \right) dt}{\int_{t_1}^{t_2} \left(C_{H_2O} \dot{N}_{H_2O,out}^{an} + C_{O_2} \dot{N}_{O_2} \right) dt} \tag{15}$$

Subtracting t_1 from t_2 represents the time during which the gas-water mixture flows through the anode chamber. The heat released from the cathode into the circulating water per unit of time is:

$$\dot{Q}_{H_2O}^{cat} = C_{H_2O} \dot{N}_{H_2O,mem} (T_{out}^{cat} - T_{cell}^{an}) \tag{16}$$

The heat released into the hydrogen gas per unit of time is:

$$\dot{Q}_{H_2} = C_{H_2} \dot{N}_{H_2} (T_{out}^{cat} - T_0) \tag{17}$$

where $\dot{N}_{H_2}$ represents the molar quantity of hydrogen discharged per unit time. The heat released from the cathode per unit of time is equal to the sum of the heat in the cathode circulating water and the heat in the hydrogen gas:

$$\begin{aligned} \dot{Q}_{out}^{cat} &= \dot{Q}_{H_2O}^{cat} + \dot{Q}_{H_2} \\ &= (C_{H_2O} \dot{N}_{H_2O,mem} + C_{H_2} \dot{N}_{H_2}) (T_{cell}^{cat} - T_0) \end{aligned} \tag{18}$$

where C_{H_2} represents the molar heat capacity of hydrogen gas, and T_{cell}^{cat} represents the cathode temperature of the electrolyzer. The expression for the average cathode temperature is:

$$T_{cell}^{cat} = \frac{\int_{t_3}^{t_4} \left(\dot{Q}_{all}^{cat} - \dot{Q}_{out}^{cat} \right) dt}{\int_{t_3}^{t_4} \left(C_{H_2O} \dot{N}_{H_2O,mem} + C_{O_2} \dot{N}_{H_2} \right) dt} \tag{19}$$

The subtraction of t_3 from t_4 represents the time during which the gas-water mixture flows through the cathode chamber.

2) CALCULATION OF ENERGY LOSS IN PIPING

The boundary conditions for the experimental model and heat transfer in the pipeline are such that T_{wg}^{cat} and T_{wg}^{an} represent the temperatures of the cathode and anode steam-water mixtures, respectively, and the average temperature of the cathode and anode in the PEM electrolysis cell is approximated to represent the temperature of the steam-water mixture in the outlet pipelines of both electrodes:

$$\begin{cases} T_{wg}^{cat} = T_{cell}^{cat} \\ T_{wg}^{an} = T_{cell}^{an} \end{cases} \tag{20}$$

Energy transfer occurs through three forms: conduction, convection, and radiation. Due to water's significantly higher thermal conductivity compared to that of gas, the heat lost

in the pipes mainly considers three aspects: convective heat transfer between the circulating water and the pipe inner wall, convective heat transfer between the pipe outer wall and the surrounding environment, and their thermal resistances are respectively represented by R_{tr1}, R_{tr2}, and R_{tr3}. The total heat transfer coefficient K_p of the pipeline for the pipeline liquid and the external temperature difference of 1 °C, the unit time through the unit heat transfer area of the heat, used to describe the degree of heat dissipation in the pipeline, approximated by heat balance equation:

$$K_p = \frac{1}{R_{tr1} + R_{tr2} + R_{tr3}} = \frac{1}{\frac{1}{2\pi r_1 \alpha_1} + \frac{1}{2\pi r_2 \alpha_2} + \frac{\ln(r_2/r_1)}{2\pi \lambda_1}} = \frac{2\pi}{\frac{1}{r_1\alpha_1} + \frac{1}{r_2\alpha_2} + \frac{\ln(r_2/r_1)}{\lambda_1}} \tag{21}$$

where α_1 represents the convective heat transfer coefficient between the circulating water and the pipe wall, α_2 represents the convective heat transfer coefficient between the pipe wall and the air, λ_1 is the thermal conductivity of the pipe wall, and the inner and outer diameters of the pipe are denoted by r_1 and r_2 respectively. However, the calculations for α_1, α_2, and λ_1 can be quite complex. The actual calculation of the heat transfer coefficient of the pipe wall can be reversed according to the Schukhov's equation [20]:

$$K_p = \frac{\dot{N}_{H_2O} C_{H_2O}}{\pi r_2 L_p} \cdot \ln \frac{T_{p,ini} - T_0}{T_{p,end} - T_0} \tag{22}$$

where L_p is the measured length of the pipe, $T_{p,ini}$ and $T_{p,end}$ are the water temperatures at the starting and ending points, and T_0 is the external temperature of the pipe. The heat lost from the pipe per unit time is given by:

$$\begin{cases} \dot{Q}^{an}_{pipe,loss} = K_{p1}(T^{an}_{wg} - T_0)\pi r_2 L_{r1} \\ \dot{Q}^{cat}_{pipe,loss} = K_{p2}(T^{cat}_{wg} - T_0)\pi r_2 L_{r2} \end{cases} \tag{23}$$

The sum of the heat lost from the pipe and the heat lost from the gas represents the heat loss of the anode and cathode. According to Joule's law, this heat loss can be equivalently represented as a resistance:

$$\begin{cases} \dot{Q}^{an}_{loss} = \dot{Q}^{an}_{pipe,loss} + \dot{Q}_{O_2} = I^2_{cell} R^{an}_{hl} \\ \dot{Q}^{cat}_{loss} = \dot{Q}^{cat}_{pipe,loss} + \dot{Q}_{H_2} = I^2_{cell} R^{cat}_{hl} \end{cases} \tag{24}$$

where R^{cat}_{hl} and R^{an}_{hl} represent the equivalent resistance of heat losses at the cathode and anode, respectively, and their corresponding voltages are U^{cat}_{hl} and U^{an}_{hl}, the total voltage in the engineering model is:

$$U_{cell} = U_{rev} + U_{act.c} + U_{act.a} + U_{ohm} + U_{hl} \tag{25}$$

The PEM engineering model is depicted in Fig. 4. Since heat loss is considered external to the PEM electrolyzer, the model is divided into two parts: the internal equivalent circuit and an additional resistance for external heat loss, referred to as the "additional resistance" in the following text.

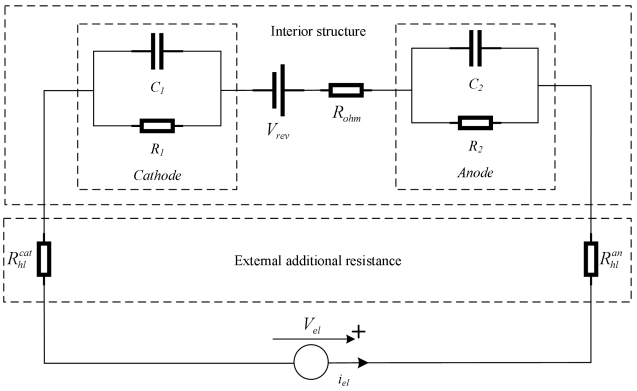

FIGURE 4. PEM electrolyzer engineering model.

III. IDENTIFICATION OF EQUIVALENT CIRCUIT PARAMETERS INSIDE THE PEM ELECTROLYZER ENGINEERING MODEL

With changes in operating conditions, the physical and electrochemical characteristics of the PEM electrolyzer change, and the parameters in the equivalent circuit model change accordingly. In practical engineering, the parameters of the equivalent circuit of the PEM electrolyzer are not directly measurable. To accurately predict and control the behavior of a PEM electrolyzer, identifying the parameters in the equivalent circuit model is a prerequisite.

Since heat losses are external energy losses in the PEM electrolyzer, the parameter identification in this paper is divided into two parts for the engineering model: first, the identification of the internal second-order RC circuit, followed by curve fitting to obtain the functional relationship between current and external additional resistance.

A. ESTABLISHING THE SECOND-ORDER RC CIRCUIT STATE EQUATION

The state equation accurately describes the relationship between system inputs and states and serves as the raw form required for recursive algorithms. Therefore, in this section, we establish a state equation to represent the relationship between the state and properties of the PEM electrolyzer. Fig. 5 shows the polarization curve obtained through MATLAB simulation of the PEM electrolyzer. The total voltage of the electrolyzer is composed of reversible voltage, ohmic overvoltage, and activation overvoltage. From the graph, it can be observed that ohmic overvoltage is directly proportional to current density, while the reversible voltage gradually decreases with an increase in the electrolyzer's temperature, although the decrease is not very pronounced. The dynamic characteristics of the equivalent circuit of the PEM electrolyzer are mainly caused by the double-layer effect at the cathode and anode, where the electrodes are separated from the electrolyte surface charge to form a double-layer of equal amount and opposite sign. In Fig. 5, it takes a certain amount of time for the cathode and anode activation overpotential curves to reach saturation. This time delay is represented by the time constant τ, which can be

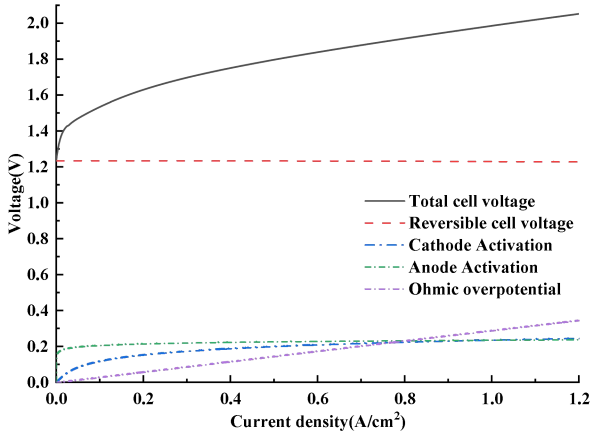

FIGURE 5. Polarization curves of PEM electrolyzer and overpotentials of each section.

approximated as the product of resistance and capacitance, i.e., $\tau = R \times C$ [13].

In the equivalent circuit, the use of cathode and anode capacitances, C_1 and C_2, simulates the double-layer effects at the cathode and anode of the electrolyzer. R_1 represents the cathode heat loss, while R_2 models the Gibbs free energy and heat loss at the anode. These components collectively account for the dynamic behavior of the PEM electrolyzer [8]. The state equation for the activation overvoltage at the cathode and anode can be derived from Kirchhoff's current law:

$$\begin{cases} \dfrac{dU_{act.c}}{dt} = \dfrac{i_{el}}{C_1} - \dfrac{U_{act.c}}{\tau_1} \\ \dfrac{dU_{act.a}}{dt} = \dfrac{i_{el}}{C_2} - \dfrac{U_{act.a}}{\tau_2} \end{cases} \tag{26}$$

The output equation is given by:

$$U_{cell} = U_{rev} + U_{act.c} + U_{act.a} + R_{ohm} \times i_{el} \tag{27}$$

Let $U_{cell.1} = U_{cell} - U_{rev}$, and express the state equation and output equation in matrix form:

$$\begin{cases} \begin{bmatrix} \dot{U}_{act.c} \\ \dot{U}_{act.a} \end{bmatrix} = \begin{bmatrix} -\frac{1}{\tau_1} & 0 \\ 0 & -\frac{1}{\tau_2} \end{bmatrix} \begin{bmatrix} U_{act.c} \\ U_{act.a} \end{bmatrix} + \begin{bmatrix} \frac{1}{C_1} \\ \frac{1}{C_2} \end{bmatrix} i_{el} \\ U_{cell.1} = \begin{bmatrix} 1 & 1 \end{bmatrix} \begin{bmatrix} U_{act.c} \\ U_{act.a} \end{bmatrix} + R_{ohm} i_{el} \end{cases} \tag{28}$$

Denote the matrices A, b, c, and d as:

$$A = \begin{bmatrix} -\dfrac{1}{\tau_1} & 0 \\ 0 & -\dfrac{1}{\tau_2} \end{bmatrix}, \; b = \begin{bmatrix} \dfrac{1}{C_1} \\ \dfrac{1}{C_2} \end{bmatrix}, \; c = \begin{bmatrix} 1 & 1 \end{bmatrix}, \; d = R_{ohm}$$

B. EQUATION OF STATE DISCRETIZATION AND DIFFERENTIAL DIFFERENTIATION

Since computers can only process discrete digital signals, it is necessary to discretize the state equations established in (28) and convert them into a different equation form suitable for recursive algorithms. When sampling a system, it is necessary to convert a continuous-time system into a discrete-time system by transforming the continuous-time variable "t" into a discrete-time variable "k." This transformation represents the variable at discrete time instances " $t = kT$," where "T" is the sampling period. Using a zero-order hold discretization method, denoted as $U_{act}(t) = U_{act}(kT), kT \le t < (k+1)T$, and designated as $U_{act}(kT) = U_{act}(k)$.

In our approach, a crucial assumption is introduced, where within the short time intervals employed for analytical time integration, the resistances R_1 and R_2 (representing anode and cathode resistances) and capacitances C_1 and C_2 (representing anode and cathode capacitances) of the second-order RC circuit are presumed to remain constant. Specifically, at each time step T representing the sampling interval, it is assumed that these parameters do not change.

The rationale behind this assumption is grounded in our observation of the system's dynamics, indicating that variations in circuit parameters are considered negligible within these brief time intervals. Consequently, we treat both the resistance and capacitance as constants throughout the analytical time integration process. This choice is made with the intention of balancing computational efficiency and accurately capturing the dynamic behavior of the system.

The discrete-time counterpart of the continuous-time state equation is given by [24]:

$$\begin{cases} U_{act}(k+1) = G \cdot U_{act}(k) + f \cdot i_{el}(k) \\ U_{cell.1}(k) = c \cdot U_{act}(k) + d \cdot i_{el}(k) \end{cases} \tag{29}$$

The expression for the transition matrix $\Phi(t)$ is as follows:

$$\Phi(t) = e^{At} = \mathcal{L}^{-1}\left[(sI - A)^{-1}\right] = \begin{bmatrix} e^{-\frac{t}{\tau_1}} & 0 \\ 0 & e^{-\frac{t}{\tau_2}} \end{bmatrix} \tag{30}$$

This leads to the parameter matrices G and f:

$$G = e^{AT} = \begin{bmatrix} e^{-\frac{T}{\tau_1}} & 0 \\ 0 & e^{-\frac{T}{\tau_2}} \end{bmatrix} \tag{31}$$

$$\begin{aligned} f &= \int_0^T e^{At} dt \times \mathrm{B} \\ &= \begin{bmatrix} -\tau_1 e^{-\frac{t}{\tau_1}} & 0 \\ 0 & -\tau_2 e^{-\frac{t}{\tau_2}} \end{bmatrix}_{t=0}^{t=T} \times \begin{bmatrix} \frac{1}{C_1} \\ \frac{1}{C_2} \end{bmatrix} \\ &= \begin{bmatrix} \dfrac{\tau_1(1 - e^{\frac{T}{\tau_1}})}{C_1} \\ \dfrac{\tau_2(1 - e^{\frac{T}{\tau_2}})}{C_2} \end{bmatrix} \end{aligned} \tag{32}$$

Substituting G and f into (29), we obtain the discrete-time state-space equations and output equation as follows:

$$\begin{bmatrix} U_{act.c}(k+1) \\ U_{act.a}(k+1) \end{bmatrix} = \begin{bmatrix} e^{-\frac{T}{\tau_1}} & 0 \\ 0 & e^{-\frac{T}{\tau_2}} \end{bmatrix} \begin{bmatrix} U_{act.c}(k) \\ U_{act.a}(k) \end{bmatrix}$$

$$+\begin{bmatrix} \dfrac{\tau_1(1-e^{\frac{T}{\tau_1}})}{C_1} \\ \dfrac{\tau_2(1-e^{\frac{T}{\tau_2}})}{C_2} \end{bmatrix} i_{el}(k) \tag{33}$$

$$U_{cell.1}(k) = \begin{bmatrix} 1 & 1 \end{bmatrix} \begin{bmatrix} U_{act.c}(k) \\ U_{act.a}(k) \end{bmatrix} + R_{ohm} i_{el}(k) \tag{34}$$

Transforming the state equation into a difference equation form, and utilizing the properties of the shift operator, equation (33) can be expressed at time k:

$$\begin{aligned} &\begin{bmatrix} U_{act.c}(k) \\ U_{act.a}(k) \end{bmatrix} \\ &= \begin{bmatrix} z - e^{-\frac{T}{\tau_1}} & 0 \\ 0 & z - e^{-\frac{T}{\tau_2}} \end{bmatrix}^{-1} \begin{bmatrix} \dfrac{\tau_1(1-e^{\frac{T}{\tau_1}})}{C_1} \\ \dfrac{\tau_2(1-e^{\frac{T}{\tau_2}})}{C_2} \end{bmatrix} i_{el}(k) \\ &= \begin{bmatrix} \dfrac{\tau_1 e^{\frac{T}{\tau_1}}(1-e^{\frac{T}{\tau_1}})}{C_1(ze^{\frac{T}{\tau_1}}-1)} \\ \dfrac{\tau_2 e^{\frac{T}{\tau_2}}(1-e^{\frac{T}{\tau_2}})}{C_2(ze^{\frac{T}{\tau_2}}-1)} \end{bmatrix} i_{el}(k) \end{aligned} \tag{35}$$

Substituting (35) into (34) yields:

$$\begin{aligned} &U_{cell.1}(k) \\ &= \left(\frac{\tau_1 e^{\frac{T}{\tau_1}}(1-e^{\frac{T}{\tau_1}})}{C_1(ze^{\frac{T}{\tau_1}}-1)} + \frac{\tau_2 e^{\frac{T}{\tau_2}}(1-e^{\frac{T}{\tau_2}})}{C_2(ze^{\frac{T}{\tau_2}}-1)} + R_{ohm}\right) \times i_{el}(k) \end{aligned} \tag{36}$$

Let $e^{\frac{T}{\tau_1}} = a_1$ and $e^{\frac{T}{\tau_2}} = a_2$, and substitute them into (36) to obtain (37), as shown at the bottom of the next page.

Let K1-K5 be the following values (38), as shown at the bottom of the next page.

Substituting (38) into (37) gives the difference form of voltage:

$$\begin{aligned} U_{cell.1}(k) = {} & K_1 U_{cell.1}(k-1) - K_2 U_{cell.1}(k-2) \\ & + K_3 i_{el}(k) + K_4 i_{el}(k-1) + K_5 i_{el}(k-2) \end{aligned} \tag{39}$$

In equation (39), $U_{cell.1}(k)$, $U_{cell.1}(k-1)$, and $U_{cell.1}(k-2)$ represent the difference between the electrolyzer voltage and reversible voltage at time k, k−1, and k−2, respectively. $i_{el}(k)$, $i_{el}(k-1)$, and $i_{el}(k-2)$ represent the electrolyzer current at time k, k−1, and k−2, respectively.

C. MULTI-INNOVATION LEAST SQUARES (MILS) PARAMETER IDENTIFICATION

Parameter estimation algorithms can be categorized into one-shot completion algorithms, recursive algorithms, and iterative algorithms. In the online identification process, the one-shot completion algorithm utilizes all available data for parameter estimation. However, as new data emerges, the computational load gradually increases, making it less suitable for real-time applications. Recursive algorithms, on the other hand, continuously adjust estimates based on existing data and are well-suited for online identification. In contrast, iterative algorithms involve multiple rounds of parameter updates and optimization, leading to higher computational complexity and potentially requiring multiple iterations to converge. Recursive algorithms are better suited for online identification, while iterative algorithms are more adept at handling convergence issues in offline identification, unaffected by real-time system stability concerns. Therefore, this study employs the MILS algorithm for the identification of internal circuit parameters.

The PEM electrolytic cell involves electrochemistry, thermodynamics, fluid dynamics, and other disciplines. The internal equivalent circuit parameters of the cell change with variations in input electrical energy, temperature, pressure, and other state variables. To determine the values of parameters within the "black box", it is necessary to collect observational data from the system, which includes input and output data. The current moment's parameter values can be obtained through a recursive method. The additional input autoregressive model (ARX) is expressed as follows [24]:

$$\begin{cases} A(z)y(k) = B(z)u(k) + v(k) \\ A(z) = 1 + a_1 z^{-1} + a_2 z^{-2} + \cdots + a_{na} z^{-na} \\ B(z) = 1 + b_1 z^{-1} + b_2 z^{-2} + \cdots + b_{nb} z^{-nb} \end{cases} \tag{40}$$

where $y(k)$ is the system output sequence, $u(k)$ is the system input sequence, $v(k)$ is zero-mean Gaussian random white noise, and $A(z)$ and $B(z)$ are delay operator polynomials, respectively. The ARX form of the PEM electrolyzer can be obtained by (39):

$$\begin{cases} y(k) = \varphi^{\mathrm{T}}(k)\theta(k) + v(k) \\ \varphi(k) = [U(k-1), U(k-2), I(k), I(k-1), I(k-2)] \\ \theta = [K_1, K_2, K_3, K_4, K_5] \end{cases} \tag{41}$$

where $\varphi(k)$ is an information vector consisting of input current and output voltage data, θ is a parameter to be recognized, and $v(k)$ is a scalar new interest, which can be expressed as:

$$v(k) = y(k) - \varphi^{\mathrm{T}}(k)\hat{\theta}(k-1) \tag{42}$$

Extend innovation scalar to innovation vectors:

$$V(p,k) = \begin{bmatrix} y(k) - \varphi^{\mathrm{T}}(k)\hat{\theta}(k-1) \\ y(k-1) - \varphi^{\mathrm{T}}(k-1)\hat{\theta}(k-1) \\ \vdots \\ y(k-p+1) - \varphi^{\mathrm{T}}(k-p+1)\hat{\theta}(k-1) \end{bmatrix} \tag{43}$$

where p is the innovation length. In order to be compatible with the dimensionality of matrix multiplication, the information vector $\varphi(k)$ should also be extended to the corresponding

matrix:

$$\phi(p,k)=\begin{bmatrix}\varphi(k)\\ \varphi(k-1)\\ \vdots\\ \varphi(k-p+1)\end{bmatrix} \tag{44}$$

Then the system multi-innovation least squares identification algorithm is of the form:

$$Y(p,k)=\phi^{\mathrm{T}}(p,k)\theta(k-1)+V(p,k) \tag{45}$$

The recursive procedure for updating the parameters of the MILS algorithm can be obtained after derivation [25]:

$$\hat{\theta}(k)=\hat{\theta}(k-1)+L(k)[Y(p,k)-\phi^{\mathrm{T}}(k)\hat{\theta}(k-1)] \tag{46}$$

$$L(k)=P(k-1)\phi(p,k)(I_p+\phi^{T}(p,k)P(k-1)\phi(p,k))^{-1} \tag{47}$$

$$P(k)=P(k-1)-L(k)\phi^{T}(p,k)P(k-1) \tag{48}$$

In equations (46), (47), and (48) represent the parameter update equation, gain update equation, and covariance matrix update equation, where $\hat{\theta}(k)$ and $\hat{\theta}(k-1)$ are the current and previous parameter estimates, $L(k)$ is the gain vector, and $P(k)$ is the covariance matrix. The detailed MILS algorithm flow can be found in APPENDIX A.

IV. PEM ELECTROLYZER ENGINEERING MODEL EXTERNAL ADDITIONAL RESISTANCE PARAMETER FITTING

Section B in part II analyze the heat lost from the cathode and anode gases in the PEM electrolyzer and the heat lost from the pipeline heat transfer, respectively. It provides a method to equivalently represent the heat losses at the anode and cathode as resistances, where the heat in the gas at the anode and cathode is determined by (12) and (16), and the heat lost through circulating water in the pipes is determined by (23). The total heat loss in the PEM electrolyzer is obtained by adding the heat from the gas and the heat losses from the pipes. Subsequently, the additional impedance is reverse-calculated using (24). Because the additional impedance tends to stabilize with the current, as shown in Fig. 6, the anode and cathode additional resistances gradually stabilize under a step current of 160A. Therefore, in this study, the additional resistances at steady currents ranging from 20A to 200A were obtained through simulation experiments. These resistances were then fitted to functions of current using curve fitting methods.

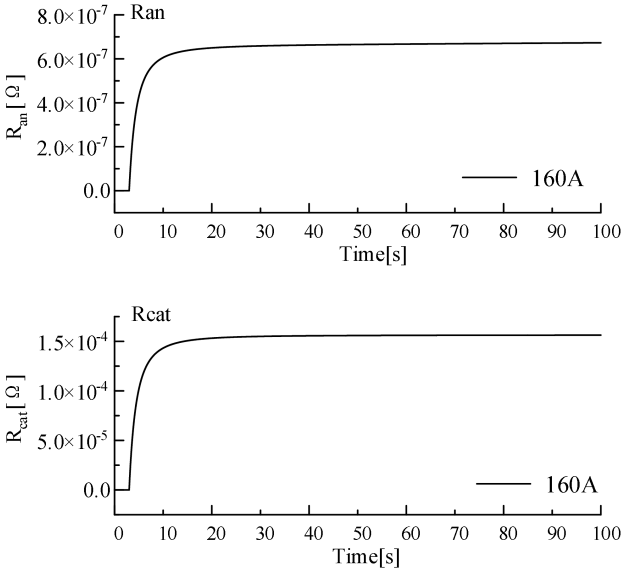

FIGURE 6. Trend of additional resistance at 160A step current.

The power supply for the PEM electrolyzer is typically obtained from renewable energy through AC/DC or DC/DC converters for rectification and voltage reduction. The resulting current waveform is generally a constant direct current (DC), and when the power from renewable sources changes, the DC current undergoes corresponding step changes. To determine the values of additional resistance

$$U_{cell.1}(k)=\left(\frac{z^2R_3+z\frac{C_1\tau_2a_1a_2+C_2\tau_1a_1a_2-C_1\tau_2a_1a_2^2-C_2\tau_1a_1^2a_2-C_1C_2R_3a_1-C_1C_2R_3a_2}{C_1C_2a_1a_2}}{z^2-z\frac{(a_1+a_2)}{a_1a_2}+\frac{1}{a_1a_2}}+\frac{\frac{C_2\tau_1a_1^2-C_1\tau_2a_2-C_2\tau_1a_1+C_1\tau_2a_2^2+C_1C_2R_3}{C_1C_2a_1a_2}}{z^2-z\frac{(a_1+a_2)}{a_1a_2}+\frac{1}{a_1a_2}}\right)i_{el}(k) \tag{37}$$

$$\begin{cases}K_1=\dfrac{(a_1+a_2)}{a_1a_2}\\ K_2=\dfrac{1}{a_1a_2}\\ K_3=R_3\\ K_4=\dfrac{C_1\tau_2a_1a_2+C_2\tau_1a_1a_2-C_1\tau_2a_1a_2^2-C_2\tau_1a_1^2a_2-C_1C_2R_3a_1-C_1C_2R_3a_2}{C_1C_2a_1a_2}\\ K_5=\dfrac{C_2\tau_1a_1^2-C_1\tau_2a_2-C_2\tau_1a_1+C_1\tau_2a_2^2+C_1C_2R_3}{C_1C_2a_1a_2}\end{cases} \tag{38}$$

TABLE 1. PEM electrolytic cell system main parameter Settings.

Parameters	Abbreviation	Values
Membrane area	A	$160cm^2$
Membrane thickness	δ_m	$0.0254cm$
Cathode volume	V_{cat}	$0.064m^3$
Anode volume	V_{an}	$0.064m^3$
Cathode charge transfer coefficient	α_{cat}	0.5
Anode charge transfer coefficient	α_{an}	2
Cathode exchange current density	$J_{0,cat}$	$1\times10^{-3}\,A/cm^2$
Anode exchange current density	$J_{0,an}$	$1\times10^{-9}\,A/cm^2$
Cathode pressure	P_{H_2}	$4.868bar$
Anode temperature	T_{cell}^{an}	$308K$
Cathode temperature	T_{cell}^{cat}	$338K$
Hydrogen production	$\dot{N}_{H_2}$	$8.291\times10^{-4}\,mol/s$
Current density	i	$1A/cm^2$

TABLE 2. Physical constant.

Parameters	Abbreviation	Values
Faraday constant	F	$96485C/mol$
Gas universal constant	R	$8.3145J/(mol\cdot k)$

TABLE 3. Other parameters.

Parameters	Abbreviation	Values
Overall heat transfer coefficient	K_p	$4.5W/(m\cdot k)$
Pipeline length	L_p	$80cm$
Environmental temperature	T_0	$298.15K$
Water flow rate	$\dot{N}_w$	$0.3mol/s$

under different step currents, we employed a curve-fitting method to fit the curves and derive the additional resistance values for different step currents.

At a certain moment when the input current undergoes a step change, the temperatures of the cathode and anode of the PEM electrolyzer can be determined based on the heat calculation equations (11)-(19). Using the boundary condition in (20), the temperature of the entire electrolyzer is assumed to be the temperature of the steam-water mixture. Subsequently, heat loss is calculated through (23), and the current at this moment is substituted into Equation (24) to obtain the additional impedance. The specific steps for fitting the additional resistance are as follows [23]:

1) Due to the PEM electrolyzer's maximum current capacity of 200A, we conducted simulations to gather additional impedance corresponding to currents ranging from 20A to 200A. Using current as the x-axis and additional impedance as the y-axis, we obtained a two-dimensional dataset $[x_1, y_1], [x_2, y_2], \cdots, [x_n, y_n]$.

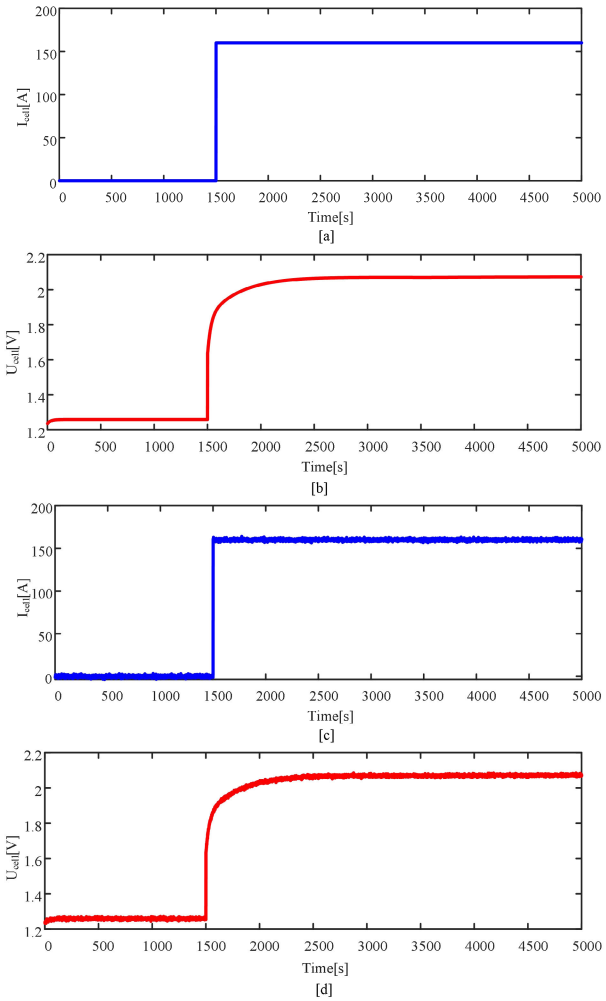

FIGURE 7. Voltage variation curve under step current input.

2) Determine the fitting function: Based on the pattern of the dataset, establish an appropriate fitting function. Since the dataset closely follows a power-law function, a power-law function is selected as the fitting function in this chapter.

$$g(x) = a \cdot x^b \tag{49}$$

3) Determine the criteria: Establish the criteria for fitting error, utilizing the least squares approach to minimize the distance between all data points and the fitted curve.

$$L(a, b) = \min \frac{1}{2} \sum_{i=1}^{n} (ax_i^b - y_i)^2 \tag{50}$$

4) Optimize Fitting Parameters: Since the criterion function is nonlinear, a numerical algorithm is needed to iteratively search for the optimal parameters a and b to minimize the criterion function.

5) Evaluate Fitting Quality: After obtaining the parameters through fitting, the quality of the fit can be assessed using evaluation metrics such as the coefficient of determination (R-squared), root mean square error (RMSE), and other relevant indicators.

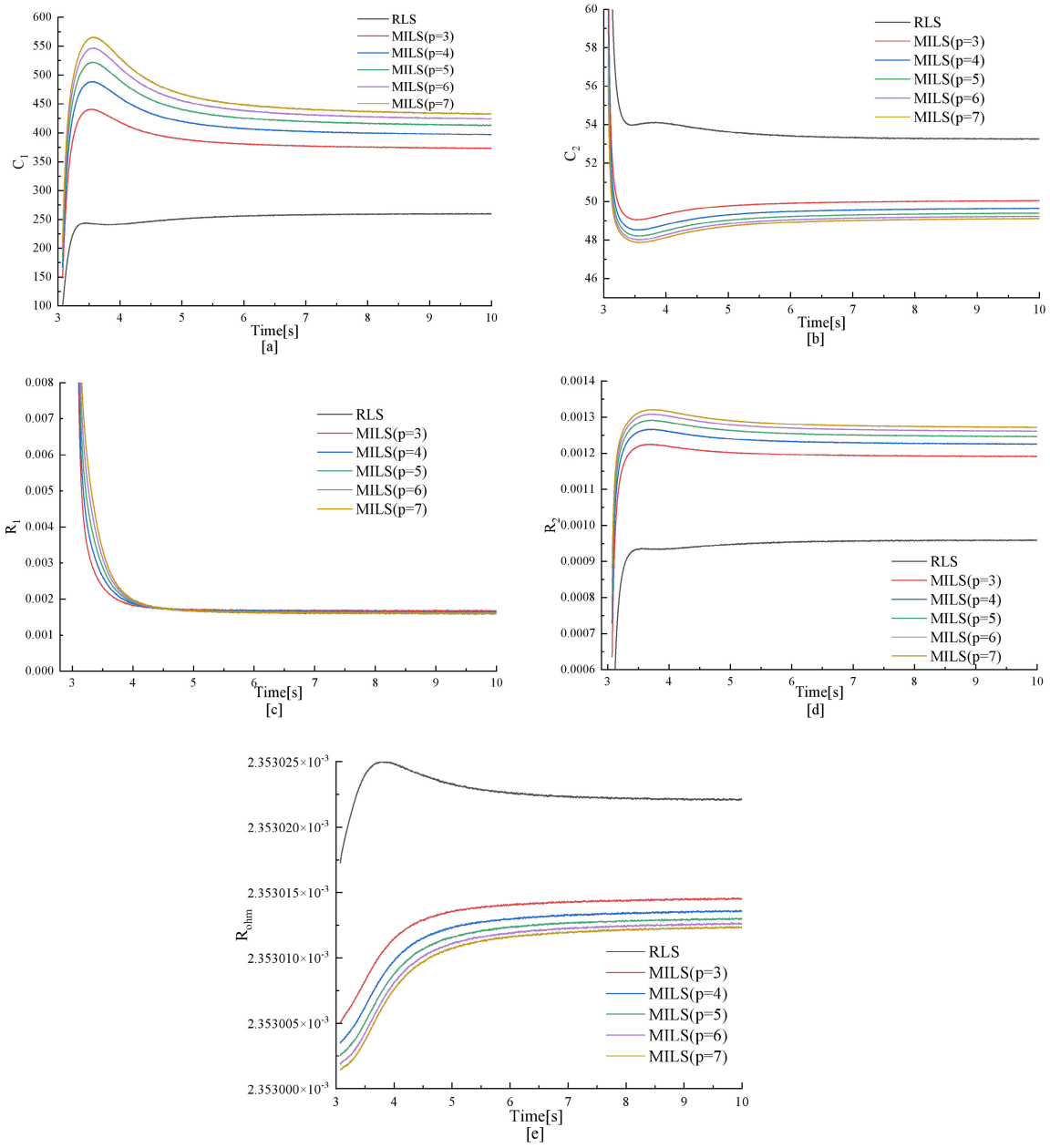

FIGURE 8. Identification results of C1, C2, R1, R2 and Rohm parameters.

The specific optimization process can be found in APPENDIX B.

V. SIMULATION VERIFICATION

This chapter extensively surveyed the parameters of existing PEM electrolyzers on the market and referenced a significant amount of literatures [1], [12], [13], and [21]. Based on this, we constructed a PEM electrolyzer engineering model as described in Chapter II, employing the MATLAB/Simulink simulation tool as a reference for the identification results. The main parameters, physical constants, and other parameters of the electrolysis cell are listed in Table 1, Table 2, and Table 3, respectively.

This chapter begins with the identification of the experimental model. Observational data from the model is collected and used in the recursive algorithm to estimate the circuit parameters of the constructed PEM electrolyzer. The overall error in the identified parameters is analyzed. Then, the additional resistance in the engineering model is curve fitted. Using Joule's law, we calculate the equivalent resistance for thermal losses within the specified current range, resulting in the derivation of the parameters for the engineering model's equivalent circuit. Finally, the simulation results of the experimental and engineering models are analyzed for errors with the identification results.

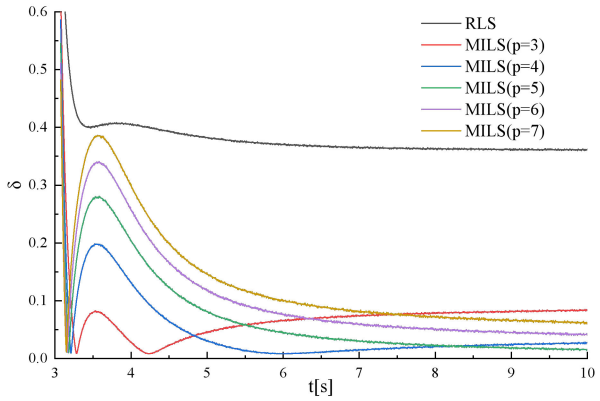

FIGURE 9. The curve of the parameter estimation error δ changing with time t.

TABLE 4. Comparison of identification results and errors for various parameters at the end of the simulation.

	RLS	MILS(p=3)	MILS(p=4)	truth-value
C_1	259.176	373.825	396.908	407.4
C_2	53.325	50.046	49.640	45.94
R_1	0.001886	0.001670	0.001639	0.001488
R_2	0.000959	0.001191	0.001225	0.001319
R_{ohm}	0.002352	0.002353	0.002353	0.002275
τ_1	0.489514	0.62341	0.65041	0.606
τ_2	0.048951	0.05961	0.06083	0.0606
δ	36.65%	8.82%	3.07%	-
	MILS(p=5)	MILS(p=6)	MILS(p=7)	truth-value
C_1	411.424	422.960	431.651	407.4
C_2	49.417	49.252	49.134	45.94
R_1	0.001621	0.001608	0.001598	0.001488
R_2	0.001245	0.001260	0.001271	0.001319
R_{ohm}	0.002353	0.002353	0.002350	0.002275
τ_1	0.66691	0.68000	0.68983	0.606
τ_2	0.06153	0.06205	0.00624	0.0606
δ	1.30%	3.88%	5.97%	-

A. IDENTIFICATION OF EQUIVALENT CIRCUIT PARAMETERS INSIDE PEM ELECTROLYZER ENGINEERING MODELS

A continuous excitation signal refers to an input signal that excites the essential characteristics of a system. To elicit the dynamic characteristics of the PEM electrolyzer, a step current excitation is applied to the system, as shown in Fig. 7(a) The simulation time is 10 seconds, with a sampling time of 0.002 seconds. The current undergoes a sudden change from 0.01A to 160A at 3 seconds. The system voltage is depicted in Fig. 7(b). Considering the presence of sensor errors, electronic component noise, measurement inaccuracies, environmental disturbances, etc., in practical systems, it is necessary to filter the collected data before parameter identification. The signal after filtering has a smaller noise compared to the original signal. Therefore, in this study, white noise is added to the ideal data to approximate the filtered data, simulating the random errors in the system. As the PEM electrolyzer cell operates with high current and low voltage, white noise sequences with mean 0 and variances of $\sigma^2 = 1$ and $\sigma^2 = 0.00002$ are added to the input data (i_{el}) and output data (u_{el}), respectively. The signal-to-noise ratios are 45.57dB and 49.14dB for current and voltage, respectively. The system currents and voltages after adding noise are shown in Fig. 7(c) and Fig. 7(d), respectively. All current and voltage data collected during the simulation period are used for parameter estimation of the PEM electrolyzer, following the identification method outlined in part III.

Based on Section B in III, it can be concluded that the difference equation of the system to be identified are represented by (39). In order to assess the effect of the innovation length on the identification process in the MILS algorithm, the innovation length (p) is set to be 3, 4, 5, 6, and 7, respectively. Additionally, the least squares method is employed as a control experiment. These methods are applied to identify the parameters of the equivalent circuit model for the PEM electrolyzer. A total of 5000 data points are collected within a 10-second period. At each time step, the input and output data of the system are used as inputs to the identification algorithm for recursive estimation, resulting in the direct identification results K_1, K_2, K_3, K_4, and K_5. These direct identification results, K_1 to K_5, are then used in (38) to obtain the final identification values, which are the parameters C_1, C_2, R_1, R_2, and R_{ohm} of the second-order RC equivalent circuit model. The final identification results are shown in Table 4. Through a comparison between the identification results of the equivalent circuit and the experimental simulation results, an assessment of the accuracy of parameter identification can be made. Based on Fig. 8 and Table 4, the following conclusions can be drawn:

1) Over a 10-second period, a total of 5000 data points were collected. As the number of recursive iterations increased, the error in the identification results steadily decreased and eventually stabilized.

2) With the increase in the innovation length, the identification error gradually reduced. When the innovation length reached a certain optimal value, the error minimized. If the innovation length continued to increase beyond this optimal point, the identification values started to deviate from the true values. When the innovation length in MILS is set to 5, the identification results show the least deviation from the true values.

3) When the innovation length in MILS is set to 1, it essentially becomes the Recursive Least Squares (RLS). RLS algorithm, which is similar to LSM, has a lower data utilization rate. In contrast, MILS not only utilizes the current data but also repetitively uses the past $p - 1$ data points, thereby increasing data utilization efficiency. This improvement enhances the convergence speed and identification accuracy of the algorithm.

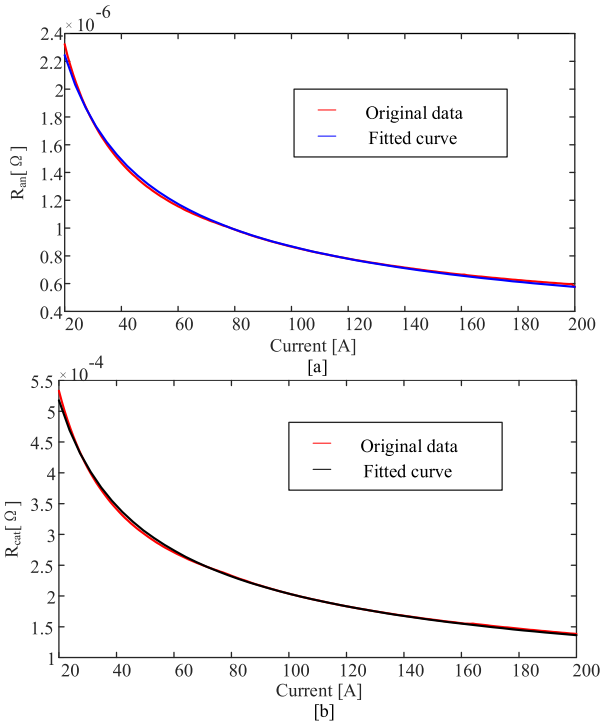

FIGURE 10. Anode and cathode R-I fitting graphs.

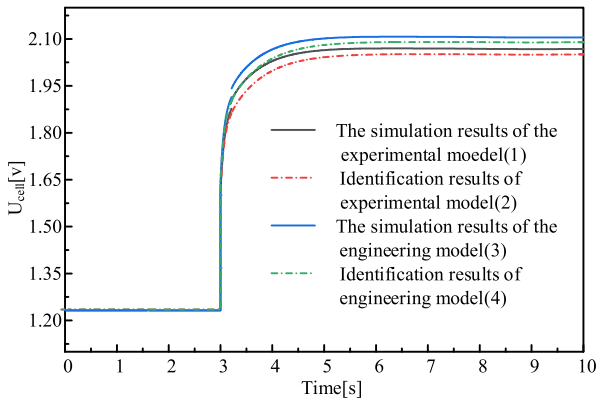

FIGURE 11. Comparison between simulation results and identification results.

Figure 9 shows the curve of parameter estimation error (δ) as a function of time (t). From this graph, it can be observed that with the innovation value of 5 in MILS (p = 5), the error tends to stabilize and reaches its minimum as time increases.

The above results indicate that representing the PEM electrolyzer experimental model as a state-space equation, transforming it into the ARX model through discretization and differencing, and then identifying it using the MILS algorithm results in an identification error of less than 2% when compared to the experimental results. This demonstrates a high level of accuracy in the identification process.

B. CURVE FITTING OF EXTERNAL ADDITIONAL RESISTANCE FOR PEM ELECTROLYZER ENGINEERING MODELS

The model established in Section B in part II allows simulating the steady-state values of cathode and anode additional resistances for different step current values, and then fitted into an R-I function. The fitted curves for anode additional impedance versus current are shown in Fig. 10[a], while the fitted curves for cathode additional impedance versus current are displayed in Fig. 10[b]. It can be observed that as the current increases, the thermal loss equivalent resistance gradually decreases. This is because even though the heat loss from the pipeline and gas loss increases with the current, the square of the current growth rate in (24) is much higher than the growth rate of thermal loss in the PEM electrolyzer, hence the decreasing trend of the additional resistance changes from sharp to slow.

This article uses nonlinear least squares to fit a power function curve, denoted as $f(x) = ax^b$. The curve depicting the change in anode and cathode additional resistances with current can be obtained as follows:

$$\begin{cases} R_{hl}^{an} = 1.3171 \times 10^{-5} \cdot x^{-0.5906} \\ R_{hl}^{cat} = 0.0029 \cdot x^{-0.5795} \end{cases} \tag{51}$$

In part IV, with an input current excitation of 160A, the fitted curve equations were applied to obtain the equivalent resistances for the anode and cathode thermal losses, resulting in values of 6.57454×10^{-7} for R_{hl}^{an} (anode) and 1.53148×10^{-4} for R_{hl}^{cat} (cathode).

C. ERROR ESTIMATION OF SIMULATION RESULTS

The error is a measure of the difference between predicted values and actual values. In order to determine the effect of fit between simulation results and identification results, this study employs the Root Mean Square Error (RMSE) and Mean Absolute Error (MAE) to calculate the errors between simulated voltage and estimated voltage. Their definitions are as follows:

$$RMSE = \sqrt{\frac{1}{n}\sum_{i=1}^{n}(U_{es}^{(i)} - U_{rel}^{(i)})^2} \tag{52}$$

$$MAE = \frac{1}{n}\sum_{i=1}^{n}\left|U_{es}^{(i)} - U_{rel}^{(i)}\right| \tag{53}$$

where $U_{es}^{(i)}$ and $U_{rel}^{(i)}$ represent the estimated and actual values for the ith data point, respectively. As shown in Fig. 11, under a step current input of 160A, the voltage simulation results for the experimental model are represented by curve (1), while the voltage simulation results for the engineering model are shown by curve (2). Curve (3) corresponds to the identification results for the experimental model, and curve (4) represents the identification results for the engineering model. It can be observed that curve (1) closely matches curve (2), indicating that the identification results for the internal circuit parameters of the engineering model are relatively accurate. Similarly, curves (3) and (4) show consistent results, reflecting the good fitting performance of the engineering model's additional impedance. The difference between curve (1) and curve (3) represents the partial

pressure of heat loss resistance, indicating the voltage deviation caused by the measurement temperature deviation. The RMSE and MAE between the identification results of the experimental model and the simulation results, calculated using (52) and (53), are 2.33% and 1.72%, respectively. For the engineering model, the RMSE and MAE between the identification results and simulation results are 0.40% and 1.41%, respectively.

VI. CONCLUSION

For better understanding, this section provides a summary of all equations and calculations. Equations (1)-(10) constitute the mathematical model of a PEM electrolyzer under experimental conditions, outlining the components of the working voltage. Equations (11)-(19) involve heat-related calculations, including temperatures of water, gas products, and cathode and anode of the electrolyzer, serving as a foundation for computing heat loss in the pipeline and additional impedance. Equations (21)-(23) calculate heat loss in the pipeline, Equation (24) uses Joule's law to equate lost heat to additional impedance, and Equation (25) represents the operating voltage of the practical engineering electrolyzer, completing the establishment of the engineering model. Equations (26)-(28) transform the mathematical model into a matrix-form state-space expression. Equations (29)-(39) discretize and difference the state-space expression, converting it into a form suitable for recursive algorithms. Equations (40)-(48) involve calculations related to MILS, where input current (Iel) and output voltage (Uel) data are input into the recursive algorithm to obtain values for K1-K5. These values, K1-K5, can be derived from the identification values of circuit parameters through Equation (38), representing the parameters of the experimental model. Equations (49) and (50) represent the fitting function and criteria, and Equation (51) presents the fitting results. Combining the obtained additional impedance with the experimental model yields the engineering model of the PEM electrolyzer. Equations (54)-(61) in Appendix B detail the derivation process of curve fitting.

The paper introduces an engineering model designed for PEM electrolyzers. This model is based on the experimental model by equating the heat in the discharged gas with the heat dissipated in the pipe as additional resistances. This compensation accounts for inaccuracies in voltage due to temperature measurement deviations in the experimental model. As the parameters of the PEM electrolyzer equivalent circuit model vary with physical and electrochemical characteristics, a system identification method is employed to estimate the model parameters. Since the heat loss is an external loss of the PEM electrolyzer, the heat loss resistance is relatively independent of the parameters in the second-order RC circuit. Therefore, the engineering model is divided into two parts for identification. Firstly, the internal parameters of the second-order RC circuit are identified using a recursive algorithm. Then, the parameters of the current vs. additional resistance power function curves were fitted by nonlinear least squares fitting of the power function curves. Finally, the accuracy of the identification results is verified by calculating the error between the identification results and the simulation results using RMSE and MAE.

The simulation results show that with an MILS innovation length of 5, the internal parameter identification error is minimized at 1.3%. The RMSE and MAE for the identification of the internal equivalent circuit of the engineering model, which is equivalent to the experimental model, are 2.33% and 1.72%, respectively. After adding the additional resistances to the experimental model, the RMSE and MAE for the identification results compared to simulation results are 0.40% and 1.41%, respectively. The sources of errors in the identification of internal equivalent circuit parameters are related to factors such as the initial values, the innovation length, convergence speed of the MILS identification algorithm, and the accuracy of the state equation discretization. The errors in the identification results after adding external additional resistances are related to data quality and the choice of the fitting model.

Through the above-mentioned method, the identification of internal equivalent circuit parameters and the fitting of external additional resistances have shown promising results. The identification results exhibit minimal discrepancies when compared to the experimental results, indicating an overall successful identification process. This approach can be helpful for predicting and controlling PEM electrolyzers in engineering applications. If the parameters of the MILS identification algorithm are adjusted appropriately, and an appropriate fitting model is selected, I believe this method can accurately identify the majority of PEM electrolyzer equivalent circuit parameters.

In conclusion, the paper presents an engineering model for PEM electrolyzers, utilizing a compensation method for temperature-related voltage inaccuracies. Internal parameters are identified using a recursive algorithm, and fitting external resistances is achieved through nonlinear least squares fitting. The identified parameters exhibit minimal discrepancies with experimental results, suggesting the potential of this method for accurate prediction and control of PEM electrolyzers in engineering applications.

APPENDIX A
MILS ALGORITHM FLOW

The identification process, as shown in Fig. 12, follows these steps [25]:

1) Initialize the parameters by setting the initial values of the parameter vector $\hat{\theta}(0)$ and the covariance matrix $p(k)$ at the moment $k = 1$.

2) Collect the current and voltage observations $i_{cell}(k)$ and $U_{cell.1}(k)$, and construct the information matrix $\Phi(p, k)$ and the innovation vector $V(p, k)$.

3) Update the parameter $\theta(k)$ using (46) and calculate the gain matrix $L(k)$ and covariance matrix $P(k)$ using (47) and (48).

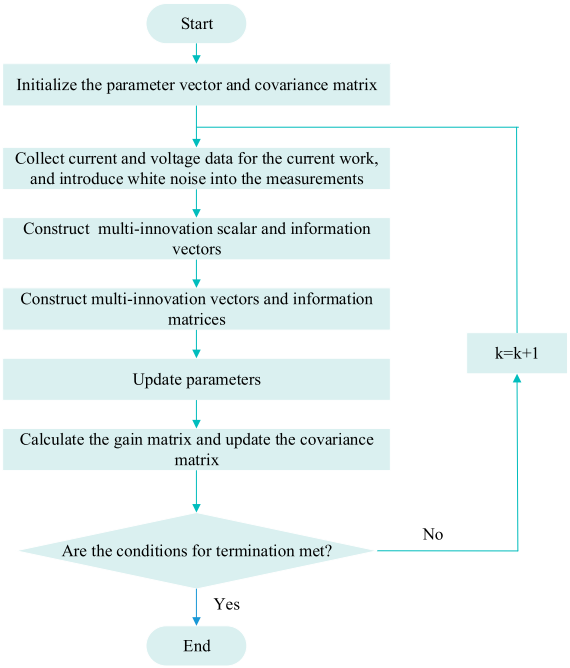

FIGURE 12. MILS algorithm process.

4) Make $K = K + 1$, determine whether the termination condition is satisfied, if $k = L$ then stop the recursion, otherwise continue the recursion.

APPENDIX B
NONLINEAR LEAST SQUARES OPTIMIZATION

The Levenberg-Marquardt (LM) algorithm combines aspects of the steepest descent and Gauss-Newton algorithms, making it a standard approach for solving nonlinear least squares problems. In this section, the LM algorithm is used for optimization in the aforementioned nonlinear problem. Let $ax_i^b - y_i = f_i(x)$ in (50) and the least squares criterion be [23]:

$$F(x) = \frac{1}{2}\sum_{i=1}^{n}(f_i(x))^2 = \frac{1}{2}\|f(x)\|^2 = \frac{1}{2}f(x)^{\mathrm{T}}f(x) \tag{54}$$

A partial derivation of the independent variables of (54) yields the least square error sum:

$$\frac{\partial F(x)}{\partial x_j} = \sum_{i=1}^{n} f_i(x)\frac{f_i(x)}{\partial x_j} \Rightarrow \nabla F(x) = F'(x) = J_f(x)^T f(x) \tag{55}$$

where $J_f(x)$ is referred to as the Jacobian matrix of $f(x)$, defined as:

$$J_f(x) = \begin{bmatrix} \frac{\partial f_1(x)}{\partial x_1} & \frac{\partial f_1(x)}{\partial x_2} & \cdots & \frac{\partial f_1(x)}{\partial x_m} \\ \frac{\partial f_2(x)}{\partial x_1} & \frac{\partial f_2(x)}{\partial x_2} & \cdots & \frac{\partial f_2(x)}{\partial x_m} \\ \vdots & \vdots & \ddots & \vdots \\ \frac{\partial f_n(x)}{\partial x_1} & \frac{\partial f_n(x)}{\partial x_2} & \cdots & \frac{\partial f_n(x)}{\partial x_m} \end{bmatrix} \in \mathbb{R}^{n\times m} \tag{56}$$

If $F(x)$ is continuous and conductible, the point at which its derivative is 0 is the extremum, i.e., the solution sought:

$$F'(x) = J_f(x)^T f(x) = 0 \tag{57}$$

Assuming there is a small increment h within the current neighborhood of x, we can use Taylor's theorem to obtain:

$$\begin{aligned} F(x+h) &= \frac{1}{2}f(x+h)^{\mathrm{T}}f(x+h) \\ &\approx \frac{1}{2}f^{\mathrm{T}}f + f^{\mathrm{T}}J_f h + \frac{1}{2}h^{\mathrm{T}}J_f^{\mathrm{T}}J_f h \end{aligned} \tag{58}$$

The LM algorithm introduces a penalty term to (58):

$$L_{lm}(h) = \frac{1}{2}f^{\mathrm{T}}f + f^{\mathrm{T}}J_f h + \frac{1}{2}h^{\mathrm{T}}J_f^{\mathrm{T}}J_f h + \frac{1}{2}\mu h^{\mathrm{T}}h,\ \mu > 0 \tag{59}$$

where μ represents the damping factor. The neighborhood size needs to be controlled when linearly approximating $f(x)$. When the approximation is good, the search neighborhood is larger, the penalty term takes a smaller proportion of $L_{lm}(h)$, μ is smaller, and the increment h is relatively large. When the approximation is poor, the search neighborhood is reduced to a smaller range, resulting in a larger μ and a smaller h. Differentiation of $L_{lm}(h)$ and setting its derivative to zero yields the increment h_{lm}:

$$\begin{aligned} L'_{lm}(h) &= J_f^{\mathrm{T}}f + (J_f^{\mathrm{T}}J_f + \mu I)h_{lm} = 0 \\ &\Rightarrow h_{lm} = -(J_f^{\mathrm{T}}J_f + \mu I)^{-1}J_f^{\mathrm{T}}f \end{aligned} \tag{60}$$

As μ approaches 0, h_{lm} tends toward the Gauss-Newton method. When μ approaches ∞, h_{lm} tends toward the small step-size steepest descent method. The approximation level of $f(x)$ is defined as follows:

$$\rho = \frac{F(x) - F(x+h_{lm})}{\frac{1}{2}h_{lm}^{\mathrm{T}}(J_f^T J_f + 2\mu I)h_{lm}} \tag{61}$$

ACKNOWLEDGMENT

The authors would like to express their appreciation to Prof. Yi-Zhi Tian for inspiring their collective interest in the development of innovative technologies. The guidance and insights provided by Prof. Tian have been invaluable to each member of their team, contributing significantly to their shared enthusiasm for this field.

REFERENCES

[1] M. B. Hossain, M. R. Islam, K. M. Muttaqi, D. Sutanto, and A. P. Agalgaonkar, "Dynamic electrical equivalent circuit modeling of the grid-scale proton exchange membrane electrolyzer for ancillary services," in *Proc. IEEE Ind. Appl. Soc. Annu. Meeting (IAS)*, Oct. 2022, pp. 1–7.

[2] G. Correa, P. Marocco, P. Muñoz, T. Falagüerra, D. Ferrero, and M. Santarelli, "Pressurized PEM water electrolysis: Dynamic modelling focusing on the cathode side," *Int. J. Hydrogen Energy*, vol. 47, no. 7, pp. 4315–4327, Jan. 2022.

[3] X. Ma, "Research status and application prospect of PEM electrolytic water to hydrogen technology_Ma Xiaofeng," *J. Sol. Energy*, vol. 43, no. 6, pp. 420–427, 2022.

[4] H. Yu, "Research progress and development proposal of hydrogen production technology from electrolyzed water," *Chin. Eng. Sci.*, vol. 23, no. 2, pp. 146–152, 2021.

[5] R. Cancelliere, A. Di Tinno, A. Cataldo, S. Bellucci, S. Kumbhat, and L. Micheli, "Nafion-based label-free immunosensor as a reliable warning system: The case of AFB1 detection in cattle feed," *Microchemical J.*, vol. 191, Aug. 2023, Art. no. 108868.
[6] O. Atlam and M. Kolhe, "Equivalent electrical model for a proton exchange membrane (PEM) electrolyser," *Energy Convers. Manage.*, vol. 52, nos. 8–9, pp. 2952–2957, Aug. 2011.
[7] D. Guilbert and G. Vitale, "Experimental validation of an equivalent dynamic electrical model for a proton exchange membrane electrolyzer," in *Proc. IEEE Int. Conf. Environ. Electr. Eng. IEEE Ind. Commercial Power Syst. Eur. (EEEIC/I&CPS Europe)*, Jun. 2018, pp. 1–6.
[8] J. Dang, F. Yang, Y. Li, X. Deng, and M. Ouyang, "Transient behaviors and mathematical model of proton exchange membrane electrolyzer," *J. Power Sources*, vol. 542, Sep. 2022, Art. no. 231757.
[9] Á. Hernández-Gómez, V. Ramirez, D. Guilbert, and B. Saldivar, "Development of an adaptive static-dynamic electrical model based on input electrical energy for PEM water electrolysis," *Int. J. Hydrogen Energy*, vol. 45, no. 38, pp. 18817–18830, Jul. 2020.
[10] B. Han, S. M. Steen, J. Mo, and F.-Y. Zhang, "Electrochemical performance modeling of a proton exchange membrane electrolyzer cell for hydrogen energy," *Int. J. Hydrogen Energy*, vol. 40, no. 22, pp. 7006–7016, Jun. 2015.
[11] R. García-Valverde, N. Espinosa, and A. Urbina, "Simple PEM water electrolyser model and experimental validation," *Int. J. Hydrogen Energy*, vol. 37, no. 2, pp. 1927–1938, Jan. 2012.
[12] Z. Abdin, C. J. Webb, and E. M. Gray, "Modelling and simulation of a proton exchange membrane (PEM) electrolyser cell," *Int. J. Hydrogen Energy*, vol. 40, no. 39, pp. 13243–13257, Oct. 2015.
[13] T. Yigit and O. F. Selamet, "Mathematical modeling and dynamic simulink simulation of high-pressure PEM electrolyzer system," *Int. J. Hydrogen Energy*, vol. 41, no. 32, pp. 13901–13914, Aug. 2016.
[14] E. Afshari, S. Khodabakhsh, N. Jahantigh, and S. Toghyani, "Performance assessment of gas crossover phenomenon and water transport mechanism in high pressure PEM electrolyzer," *Int. J. Hydrogen Energy*, vol. 46, no. 19, pp. 11029–11040, Mar. 2021.
[15] R. Khajuria, R. Lamba, and R. Kumar, "Model parameter extraction for PEM electrolyzer using honey badger algorithm," in *Proc. IEEE 3rd Int. Conf. Sustain. Energy Future Electric Transp. (SEFET)*, Bhubaneswar, India, 2023, pp. 1–6, doi: 10.1109/SeFeT57834.2023.10245702.
[16] S. Toghyani, S. Fakhradini, E. Afshari, E. Baniasadi, M. Y. A. Jamalabadi, and M. S. Shadloo, "Optimization of operating parameters of a polymer exchange membrane electrolyzer," *Int. J. Hydrogen Energy*, vol. 44, no. 13, pp. 6403–6414, Mar. 2019.
[17] R. Khajuria, R. Lamba, and R. Kumar, "Optimal parameter identification of PEM electrolyzer using bald eagle search optimization algorithm," in *Proc. IEEE 10th Power India Int. Conf. (PIICON)*, Nov. 2022, pp. 1–6.
[18] D. Guilbert and G. Vitale, "Dynamic emulation of a PEM electrolyzer by time constant based exponential model," *Energies*, vol. 12, no. 4, p. 750, Feb. 2019.
[19] F. M. Nafchi, E. Afshari, E. Baniasadi, and N. Javani, "A parametric study of polymer membrane electrolyser performance, energy and exergy analyses," *Int. J. Hydrogen Energy*, vol. 44, no. 34, pp. 18662–18670, Jul. 2019.
[20] Y. Ma, "Study on factors affecting the total heat transfer coefficient of buried pipelines," *China Petroleum Chem. Standards Qual.*, vol. 42, no. 18, pp. 139–141, 2022.
[21] V. Ruuskanen, J. Koponen, K. Huoman, A. Kosonen, M. Niemelä, and J. Ahola, "PEM water electrolyzer model for a power-hardware-in-loop simulator," *Int. J. Hydrogen Energy*, vol. 42, no. 16, pp. 10775–10784, Apr. 2017.
[22] L. Chang, S. Valyukh, T. He, Z. Chen, and Y. Yu, "Multi-surface phase-shifting algorithm using the window function fitted by the nonlinear least squares method," *J. Modern Opt.*, vol. 69, no. 3, pp. 160–171, Feb. 2022.
[23] Z. Zhu, L. You, and J. Zhang, "A review of point sets parameterization methods for curve fitting," in *Proc. 27th Int. Conf. Inf. Visualisation (IV)*, Tampere, Finland, 2023, pp. 374–377, doi: 10.1109/IV60283.2023.00070.
[24] D. Feng, "System identification (2): A basic model for system description," *J. Nanjing Univ. Inf. Eng. Natural Sci. Ed.*, vol. 3, no. 2, pp. 97–117, 2011, doi: 10.13878/J.CNKI.JNUIST.2011.02.001.
[25] D. Feng, "System identification (6): Multi-innovation identification theory and methods," *J. Nanjing Univ. Inf. Eng. Natural Sci. Ed.*, vol. 4, no. 1, pp. 1–28, 2012, doi: 10.13878/J.CNKI.JNUIST.2012.01.001.

XINKE MAO was born in Linyi, Shandong, in November 1995. He received the B.Eng. degree in electrical engineering from Tianshui Normal University, in September 2020. He is currently pursuing the master's degree in electrical engineering with Xinjiang University. His research interests include power systems and their automation, primarily involving the control of PEM electrolyzers in integrated energy systems.

YIZHI TIAN received the bachelor's degree from North China Electric Power University, Beijing, in 2010, and the master's degree from Xinjiang University, in 2014.

He has been with Xinjiang University, since 2015. He has received funding for six projects from the National Natural Science Foundation of China and one International Cooperation Project. He received funding for one project from the Autonomous Region Natural Science Foundation. Additionally, he has been involved in three industry-sponsored research projects, published ten articles, including two SCI-indexed articles and two EI-indexed articles, and holds six national invention patents. His current research interests include power system stability and control and the optimization of integrated energy systems.

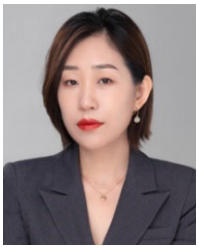

AIMEI YANG was born in Xinjiang, in August, in 1980. She received the Bachelor of Engineering degree from Xinjiang Agricultural University in 2019. Since 2015, she has been serving as the Procurement Manager at Goldwind Science and Technology Company Ltd. She has obtained certifications as a Registered Second-Class Constructor and Registered Supervision Engineer. Her research focuses on renewable energy power system generation and grid connection technology.

GAOHANG ZHANG received the Ph.D. degree in electrical power systems and automation from Xinjiang University, in 2022.

He joined the Department of Electrical Engineering and Automation, Xinjiang University, in July 2022. In 2022, he was awarded the "Tianchi Talent" Young Ph.D. Talent Program in the autonomous region. He is the Principal Investigator of one project funded by Xinjiang University's Excellent Talent Program (Class A), one project from the Autonomous Region Youth Science Fund, and one project from the Autonomous Region Graduate Student Research Innovation Program. Additionally, he is involved in one project funded by the National Natural Science Foundation of China and has contributed as a key participant in multiple research projects.